AAS 15-091

LATTICE BOLTZMANN METHOD FOR SPACECRAFT PROPELLANT SLOSH SIMULATION

Jeb S. Orr*

Joseph F. Powers†

Hong Q. Yang‡

A scalable computational approach to the simulation of propellant tank sloshing dynamics in microgravity is presented. In this work, we use the lattice Boltzmann equation (LBE) to approximate the behavior of two-phase, single-component isothermal flows at very low Bond numbers. Through the use of a non-ideal gas equation of state and a modified multiple relaxation time (MRT) collision operator, the proposed method can simulate thermodynamically consistent phase transitions at temperatures and density ratios consistent with typical spacecraft cryogenic propellants, for example, liquid oxygen. Determination of the tank forces and moments relies upon the global momentum conservation of the fluid domain, and a parametric wall wetting model allows tuning of the free surface contact angle. Development of the interface is implicit and no interface tracking approach is required. Numerical examples illustrate the method's application to predicting bulk fluid motion including lateral propellant slosh in low-g conditions.

1 INTRODUCTION

The modeling and prediction of the behavior of fluids in microgravity continues to be a challenge in the design of spacecraft systems.[1] In the microgravity environment, hydrodynamic regimes can be described by the non-dimensional parameter of Bond number (*Bo*), characterizing the relative magnitude of the gravitational acceleration versus the capillary forces present in the liquid.[2] At very low Bond numbers ($Bo < 10$), the hydrodynamics are dominated by the surface tension and a qualitative change in behavior is observed. Liquid free surface interfaces become characteristically curved, and most propellants approach a near zero contact angle with solid objects (such as tank walls). The dominant time scale of the liquid dynamics increases into the tens or hundreds of seconds, and characteristic flow velocities and the Mach number are very small ($M \ll 1$). In these conditions, computational fluid mechanics (CFM) approaches are required to predict the motion of the bulk fluid mass and its effect on the spacecraft when displaced from equilibrium.

The lattice Boltzmann equation (LBE) has recently emerged as a promising alternative to traditional approaches to computational fluid mechanics. The LBE is a method by which the continuum fluid transport phenomena, i.e. the Navier-Stokes equations, can be approximated as a solution of a discretized nonlinear difference equation based upon the kinetic theory of gases. While the LBE is

*Senior Member of the Technical Staff, The Charles Stark Draper Laboratory, Inc. (Jacobs ESSSA Group)
†Aerospace Engineer, Control Systems Design and Analysis Branch, NASA Marshall Space Flight Center
‡Senior Scientist, CFD Research Corporation (Jacobs ESSSA Group)

typically restricted to very low-velocity flows, it does provide several unique advantages over traditional solvers. First, the meshing of complex geometry is performed on a regular cartesian lattice of fluid cells, each having uniform volume in the fluid domain. As such, computations involving flux across the boundary of adjacent cells are considerably simplified. Secondly, LBE has the advantage of data locality; LBE-based flow solvers are not required to solve a global continuity equation at each time step. Finally, LBE is relatively simple to implement and computationally efficient.

In the following sections, the development of an LBE-based flow solver for spacecraft propellant dynamics will be detailed. In Section 2, the theory and basic implementation details of the LBE will be introduced. In Section 3, the method of introducing multi-phase behavior into the LBE will be discussed. In Section 4, the results of test cases that compare the outputs of the LBE flow solver with theoretical predictions will be presented. In Section 5, a summary of the present research will be provided along with some opportunities for forward work.

2 THE LATTICE BOLTZMANN METHOD

The lattice Boltzmann equation (LBE) is a discretization of the continuous Boltzmann equation, describing particle dynamics on a molecular scale. The Boltzmann equation is given by

$$\frac{\partial f}{\partial t} + \xi^T \nabla_{\mathbf{x}} f + \mathbf{a}^T \nabla_{\xi} f = \Omega(f) \tag{1}$$

where $f(\mathbf{x}, \xi, t)$ is the molecular velocity distribution function (DF) in the phase space $(\mathbf{x}, \xi)$ where $\mathbf{x} \in \mathbb{R}^D$ is the spatial position and $\xi \in \mathbb{R}^D$ is the velocity. The derivation of the Boltzmann equation follows from the statistical kinetic theory of dilute gases in a closed domain. Here, $\mathbf{a}$ is the acceleration due to the applied body force at the spatial location $\mathbf{x}$, and the collision integral is given by Ω. The right-hand side of the Boltzmann equation is the collision term describing the short-range molecular interactions of the velocity distributions assuming the modeled fluid is a dilute gas.

The direct computation of the collision operator is, in general, intractable for the continuous Boltzmann equation. However, it can be approximated by a *relaxation* operation that preserves the hydrodynamic moments that are invariants of the collision. In the simplest models, such as the BGK (Bhatnagar-Gross-Krook) approximation, the collision is approximated by a linear relaxation to the equilibrium distribution, which is related to the temperature and velocity of the flow.

The lattice Boltzmann equation follows from discretization of the $2D$-dimensional phase space and the local approximation of the resultant linear system of ordinary differential equations in discrete time, and the approximation of the equilibrium distribution function consistent with that velocity discretization. For the present model $D = 2$ and a velocity discretization of 9 directions in two dimensions is chosen. The spatial discretization is applied on a regular lattice of size δx with a temporal discretization δt. The lattice structure shown in Figure 1 is known as the D2Q9 model.

The lattice parameter $c = \delta x / \delta t$ defines the characteristic speed associated with the velocity discretization $\mathbf{e}_i$, $i = 0, 1, \ldots 8$. In this discretization, the k^{th} cell at spatial location $\mathbf{x}_k$ is described by a distribution function $\mathbf{f}(\mathbf{x}_k, t) \in \mathbb{R}^9$, the velocity distribution function at the lattice site $\mathbf{x}_k$. The i^{th} component of the discretized distribution function describes the density of particles at $\mathbf{x}_k$ having velocity $\mathbf{e}_i$. The approximation of the equilibrium distribution $\mathbf{f}^{\text{eq}}$ (namely, the Maxwell equilibrium) is carried out such that the kinetic hydrodynamic moments are consistently approximated after discretization. The continuous Maxwell distribution is expanded to third order in the velocity; the truncated equilibrium approximation then converted into a discretized form using a Gauss-Hermite

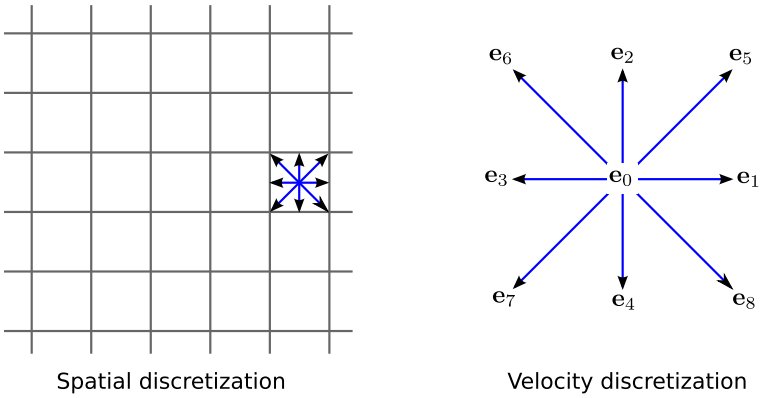

Figure 1. D2Q9 Lattice Structure

quadrature. The solution of the discretized Boltzmann equation can then be approximated by

$$\mathbf{f}(\mathbf{x}_k + \mathbf{e}\delta t, t_0 + \delta t) = \mathbf{f}(\mathbf{x}_k, t_0) - \mathbf{A}\left(\mathbf{f}(\mathbf{x}_k, t_0) - \mathbf{f}^{\mathrm{eq}}(\mathbf{x}_k, \mathbf{u}_k, \rho(\mathbf{x}_k))\right)\delta t. \tag{2}$$

where $\mathbf{u}_k$ is the local velocity and the collision matrix $\mathbf{A}$ has been introduced. The multiple scalar advection operations are implied by the operator $\mathbf{e}$ for notational convenience. The conserved hydrodynamic moments are given by

$$\rho(\mathbf{x}_k) = \sum_i f_i(\mathbf{x}_k) \tag{3}$$

$$\rho(\mathbf{x}_k)\mathbf{u}_k = \sum_i \mathbf{e}_i f_i(\mathbf{x}_k), \tag{4}$$

and the speed of sound is $c_s = c/\sqrt{3}$.

Equation 2 is the lattice Boltzmann equation. Under certain conditions, it is possible to recover the macroscopic transport and continuity equations using the Chapman-Enskog expansion of the LBE.[3] The approximation of incompressible flow is sensitive to velocity, partly due to the velocity truncation in the series expansion of the equilibrium distribution function. This implies that compressibility error is the dominant error source in the application of LBE.

The LBE is typically implemented in two steps comprising advection (streaming) and collision (relaxation) using two copies of the domain, $\mathbf{f}$ and $\mathbf{f}'$. The boundary conditions are applied at lattice sites where fluid cells are adjacent to a prescribed boundary, such as a wall. In almost all numerical implementations, the units associated with the lattice are chosen such that $\delta x = \delta t = c = 1$ and the mean density $\bar{\rho}$ is on the order of 1. This greatly reduces the computational burden and provides good numerical conditioning for the requisite computations.

In the following developments, the spatial dependency of the hydrodynamic quantities will be denoted with a subscript k for brevity, and the temporal dependency is implied.

2.1 Relaxation Operation

In implementations of the LBE using the BGK approximation, the collision matrix is replaced by a scalar *relaxation frequency* $\omega = \frac{1}{\tau}$ where τ is the relaxation time. In this single relaxation time (SRT) model, all populations relax toward equilibrium at the same rate. It has been recognized that

while the SRT model is simple to implement, the relaxation of all populations at the same rate does not allow for precise control of the higher-order kinetic moments, which leads to poor numerical stability and imprecise boundary conditions.[3,4] In order to overcome this limitation, the relaxation operation can be performed in a moment space using a suitable linear transformation $\mathbf{M}$. Stability can be markedly improved by relaxing the moments at different rates. A set of relaxation rates s_i are chosen to satisfy conservation constraints and maintain the necessary symmetry.[5]

The hydrodynamic and kinetic moments can be assembled in a vector form and a linear transformation can be derived such that $\mathbf{m} = \mathbf{M}\mathbf{f}$ where $\mathbf{M}$ is the moment matrix. The n^{th} collision operation is then performed in a moment space;

$$\mathbf{A}\left(\mathbf{f}'_k[n] - \mathbf{f}^{\text{eq}}(\mathbf{x}_k, \mathbf{u}_k, \rho_k)\right) = \mathbf{M}^{-1}\mathbf{S}\left(\mathbf{m}'_k[n] - \mathbf{m}^{\text{eq}}(\mathbf{x}_k, \mathbf{u}_k, \rho_k)\right). \tag{5}$$

Since $\mathbf{M}$ is a similarity transformation chosen to orthogonalize the modes, $\mathbf{S}$ is a diagonal matrix whose eigenvalues s_i are the relaxation parameters. In the isothermal LBE, the conserved hydrodynamic moments are only the density ρ and the momentum j_x, j_y; thus the choice of parameters s_0, s_3, and s_5 are unconstrained. The parameters $s_4 = s_6$, $s_7 = s_8$ must be equated due to symmetry and are related to the energy flux and kinematic viscosity, respectively. Finally, there is a free choice of parameters s_1 and s_2, which are related to the bulk viscosity and the energy. This scheme is known as the multiple relaxation time (MRT) model.

Usually, the choice of these parameters depends on a stability analysis conducted through linearization of the collision operator in order to determine the s_i that provide the most stable eigenvalues of the linearized LBE.[4] Alternatively, they can be selected to provide the best boundary condition accuracy. It has been shown that a proper choice of these parameters can drastically improve numerical stability of the LBE while maintaining good physical accuracy of the solution, allowing the simulation of very high Reynolds numbers in the single-phase case.[5,6]

2.2 Body Forces

The proper incorporation of external forces into the LBE is an area of active research.[7] Since the derivation of the LBE does not explicitly account for the incorporation of the acceleration term in Equation 1, various methods of incorporating these effects have been proposed.

Kupershtokh[8] devised a method to incorporate the force that simultaneously acts on the advection step and the equilibrium distribution to ensure that the entire lattice, if in local equilibrium, remains in local equilibrium after a force is applied. In this Exact Difference Method (EDM), the shift in velocity due to the applied force is first computed (with $\delta t = 1$) as $\Delta\mathbf{u}_k = \mathbf{F}_k/\rho_k$, noting that $\Delta\mathbf{u}_k = \mathbf{g}$ everywhere if a uniform acceleration is present. The lattice distribution functions are first shifted by an amount equivalent to the change in equilibrium due to this velocity increment without advection. The velocity field is then shifted and the collision is performed using the modified velocity $\mathbf{u}^\star_k$.

The computational implication of the increase in accuracy is that the equilibrium distribution must be computed at least twice. However, these steps can be combined into a single collision equation;

$$\mathbf{f}_k[n+1] = \left(\mathbf{I} - \mathbf{M}^{-1}\mathbf{S}\mathbf{M}\right)\left(\mathbf{f}'_k[n] - \mathbf{f}^{\text{eq}}(\mathbf{x}_k, \mathbf{u}_k, \rho_k)\right) + \mathbf{f}^{\text{eq}}(\mathbf{x}_k, \mathbf{u}^\star_k, \rho_k). \tag{6}$$

In our model, this mechanization provides about a 20% performance improvement over the original three-step process. In particular, the matrix $\mathbf{I}-\mathbf{M}^{-1}\mathbf{S}\mathbf{M}$ may be precomputed, saving considerable computational expense at each lattice site.

In an advanced MRT model, especially when used for multiphase flow, it is necessary to relax not only the hydrodynamic modes at different rates, but individual cells must have different effective relaxation frequencies ω_k. If this is the case, the matrix $\mathbf{A}$ can be expanded as

$$\mathbf{A}_0 + \omega_k \Delta \mathbf{A}_k = \mathbf{M}^{-1} \left(\mathbf{S}_0 + \Delta \mathbf{S}_k \right) \mathbf{M} \tag{7}$$

where $\mathbf{S}_0$ is the bulk hydrodynamic part of the collision matrix, with $s_7 = s_8 = 0$. The matrix $\Delta \mathbf{A}_k$ therefore relaxes only the diagonal and off-diagonal components of the stress tensor p_{xx} and p_{xy}, respectively. Letting $\Delta \mathbf{f}_k[n] = \mathbf{f}'_k[n] - \mathbf{f}^{\mathrm{eq}}(\mathbf{x}_k, \mathbf{u}_k, \rho_k)$, the MRT collision equation has the final form

$$\mathbf{f}_k[n+1] = \left(\mathbf{I} - \mathbf{A}_0 \right) \Delta \mathbf{f}_k[n] + \mathbf{f}^{\mathrm{eq}}(\mathbf{x}_k, \mathbf{u}^\star_k, \rho(\mathbf{x}_k)) - \omega_k \Delta \mathbf{A}_k \Delta \mathbf{f}_k[n]. \tag{8}$$

Global conservation of momentum can be used to deduce the net force on the domain, which is of primary importance for spacecraft dynamics applications. The lattice site momentum density can be used to compute the net momentum at time step n as $\mathbf{p}[n] = \sum_k \rho_k \mathbf{u}_k$; since the fluid mass and time step are equal to unity in the LBE, the net change in momentum density is equal to the internal force from Newton's law. The total domain force $\mathbf{F}_d$ is therefore the difference of the internal force and the body force;

$$\mathbf{F}_d[n] = \sum_k \mathbf{F}_k - \left(\mathbf{p}[n] - \mathbf{p}[n-1] \right). \tag{9}$$

3 MULTI-PHASE FLOW

The incorporation of multi-phase phenomena into the LBE is an emerging topic and has received much recent attention in the literature. Numerous methods for incorporating phase transitions in the LBE have been proposed.[9] These can generally be divided into two major categories of explicit and implicit interface methods. In the explicit interface methods, similar to the approaches used for Navier-Stokes codes, the two fluid species are tracked via markers or coloring methods and the interface is defined at each time step. Either mass transfer across the interface is explicitly computed, or the interface tracking is performed with level sets.

Implicit interface methods such as the Shan-Chen model[10] simulate multiple phases uniformly in the lattice via the use of a pseudopotential function which models intramolecular interactions. A real gas equation of state can be used to elicit thermodynamically consistent phase transitions, which allows direct parameterization of the temperature.[11,12] Effects such as phase separation, evaporation, and condensation occur continuously in the lattice while mass is conserved globally. This capability is particularly attractive for the modeling of cryogens, where the fluid temperature $T < T_c$ may not be extremely subcritical and phase transitions must be accurately captured.

The pseudopotential model is a diffuse interface model; that is, the interface appears in the lattice as a density gradient over a few cells or tens of cells. This increases the required minimum lattice resolution to obtain sharp interface definition if required by the application. A disadvantage of the pseudopotential model is the interdependency of the interface thickness and the surface tension parameter. In addition, high pseudopotential forces are required to maintain the interface, degrading the numerical stability.[11] Of course, the basic LBE is isothermal; convective effects, which can be

important in cryogenic flows in zero-g, are not captured.[1] However, the simplicity of implementation makes the pseudopotential model attractive in the present application insofar as it can be used to characterize bulk fluid behavior in response to transient accelerations.

3.1 Pseudopotential Model

In the formulation of a pseudopotential multiphase model based on the Shan-Chen (SC)[10] scheme, the intramolecular interaction force is related to a scalar function ψ_k that depends on the local characteristics of the lattice site. The intramolecular force can be shown to satisfy a pressure

$$p_k = \rho_k c_s^2 - \frac{c_s^2}{2}\psi_k^2. \tag{10}$$

Equation 10 describes the equation of state (EoS) for the non-ideal LBE, and has both the ideal part and the non-ideal part. A real gas equation of state $p = p(\rho)$ can be incorporated[11] if the effective mass is of the form

$$\psi_k = \sqrt{\frac{2\left(c_s^2\rho_k - p_k\right)}{c_s^2}}. \tag{11}$$

In this case, phase segregation occurs consistent with the Maxwell construction when the temperature is subcritical. The interaction potential is computed by approximating the spatial gradient on the lattice using a central finite difference scheme.[12]

While various equations of state can be incorporated into the LBE pseudopotential model through the use of Equation 11, the Carnahan-Starling EoS[13] has been widely used in the LBE due to its accuracy and numerical properties.[11] For use in the LBE, the C-S EoS is often given in the pressure-density form as

$$p = \rho RT\frac{1 + b\rho/4 + (b\rho/4)^2 - (b\rho/4)^3}{(1 - b\rho/4)^3} - a\rho^2 \tag{12}$$

The C-S EoS is parameterized by the coefficients a, b, R, and the temperature T, but unlike some other EoS, has no free parameters. That is, a, b are completely specified by the critical point conditions. Since the EoS is valid in any unit system, for proper incorporation into the LBE with $0 < \rho(\mathbf{x}_k) < 1$ the most common parameterization is to choose $a = 1$, $b = 4$, and $R = 1$.

Accuracy of the pseudopotential model can be broadly characterized into two categories: (1) accuracy of the EoS in reproducing the commonly accepted or experimental data associated with a particular gas or liquid phase of a substance, and (2) accuracy of the LBE in converging the densities to those modeled by the EoS at a particular temperature and pressure. Both affect overall solution accuracy.

A comparison with reference coexistence data for liquid oxygen was performed using the C-S EoS. The C-S EoS over-predicts the density of both the liquid and vapor phases and over-predicts the pressure. Since the simulation will be executed in isothermal and isochoric conditions, the C-S critical parameters were corrected to match the target parameters for the liquid at a specified temperature. The simulation results confirmed that the C-S EoS is only locally accurate, and still over-predicts the pressure slightly. This is a fundamental limitation in the use of a universal EoS.

3.2 Fluid-Wall Interaction

Interaction with solid boundary conditions are specified using a supplementary wall wetting model that is similar to the pseudopotential force. First, the potential function near the wall must be modified in order to reconstruct the unknown gradient near the wall. Other than when explicitly specified, it is preferred that the fluid ignore the contribution of the wall. Local modification of the effective mass function is performed such that the gradient near the wall is identically zero and a supplemental wall interaction force is applied using a boundary condition function s_k equal to one if $\mathbf{x}_k \in \partial\varphi$ and zero otherwise. The parameter G_w is the wall interaction coefficient.[14]

The contact angle can be indirectly specified by G_w, where $G_w < 0$ implies a non-wetting fluid and $G_w > 0$ implies a wetting fluid. For $G_w > 0$, the interaction potential is attractive for the higher-density liquid phase, and thus the contact angle will approach zero. For $G_w = 0$, the wall behaves as the phase in which it is immersed and the contact angle will be small. For $G_w < 0$, the lower-density vapor phase will be attracted to the wall and the contact angle will be less than π. In all cases, the wall interaction coefficient must be selected based upon the known wetting properties of the fluid under study.

3.3 Dissipation and Stability

In many implementations appearing in the literature, the stability is fundamentally limited by the kinematic viscosity of the modeled fluid, which is assumed to be uniform in the lattice. The development of instability as the density ratio is increased is usually the result of high velocities adjacent to the interface. Since the density of the vapor phase near the interface is very small, the high interface forces combined with the high-order anisotropy of the potential induce errors that lead to numerical instability.[9]

In the actual fluid, the invariant isothermal transport coefficient is the dynamic viscosity μ, and the kinematic viscosity is given by the relationship of the dynamic viscosity and the fluid density. Thus, the local relaxation rate can be modified to account for the variation in kinematic viscosity within the lattice. The local relaxation frequency is given by

$$\omega_k = \frac{2}{6\nu_k + 1} \tag{13}$$

where ν_k is the local kinematic viscosity, $\nu_k = \mu/\rho_k$. The relaxation rates are specified on a per-cell basis using the method given in Equation 8. As the vapor phase density is much lower, the kinematic viscosity of the gas is much higher than that of the liquid. This model is consistent with the physics and substantially improves the stability near the interface.

In certain applications where instabilities appear due to local density fluctuations or high Reynolds number flow, it may be appropriate to use a sub-grid turbulence scheme, such as the Smagorinsky model, to model eddy viscosity that exists at a scale smaller than can be resolved at a given lattice resolution.[15] The use of a turbulence model should be approached with caution as it must be tuned to accurately predict the physical behavior. However, the computational cost of the turbulence model with a coarse grid may be less than the fine grid required to resolve the detail, with both parameterizations yielding equivalent bulk fluid behavior.

4 IMPLEMENTATION AND EVALUATION

In the present research, all of the LBE computation, data processing, and visualization is implemented directly in MATLAB. Extensive use of MATLAB's multi-dimensional array operators allows many of the necessary operations, such as advection, collision, and the calculation of body forces, to be accomplished without the use of nested loops. By relying on MATLAB's internally optimized matrix libraries for much of the large-scale multiplication and division operations, a considerable advantage in computational efficiency and code simplicity is realized. All of the test cases detailed in this paper were run on Macintosh laptop computer with a 2.3 GHz Intel Core i7 CPU and 8 GB of 1.6 GHz DDR3 memory.

4.1 Wall Wetting Effects

Surface tension forces affecting fluid-wall interaction are important in the modeling of propellant management devices, such as traps and vanes. The behavior of the wall wetting model was investigated using a special domain containing a variety of corner geometry. The domain size is 5 cm^2 with a lattice dimension $n = 128$. The maximum relaxation frequency $\omega = 1.998$ giving a time step of $\hat{t} = 0.162$ msec with no domain acceleration. A droplet of radius 20 lattice units was placed at the center of the domain and the sensitivity to G_w was determined.

The results are shown in Figure 2. As the wall interaction potential becomes positive, the contact angle decreases and the fluid strongly adheres to acute corners. However, for $G_w > 0.1$ and $G_w < -0.5$ a sharp increase in spurious velocities is noted, possibly due to the sharp gradients near the corners. In addition, for positive values of G_w the fluid is attracted to the wall, creating a nonuniform density near the wall due to the local compressibility error.

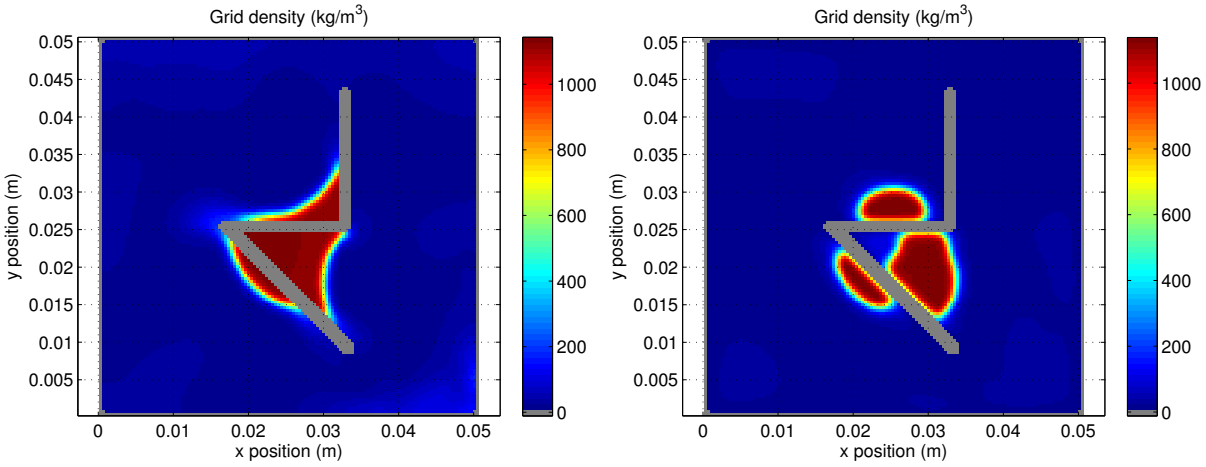

Figure 2. Sensitivity to wetting model parameter (left, $G_w = 0$, right, $G_w = -0.5$)

The use of $G_w < 0$, as expected, produces a hydrophobic wall and increases the contact angle to $\pi/2$ or greater. No impacts to stability are observed for small values of G_w. For large negative values of G_w, the wall is strongly hydrophobic and a low-density layer will form between the droplet and the wall.

4.2 Lateral Sloshing

Lateral sloshing dynamics are a fundamental concern for control system stability in rocket-propelled space vehicles. Analytical solutions for lateral slosh motion in an axisymmetric container can be derived for a variety of conditions; the simplest case describes a container in a high-g condition where the free surface height h is greater than the diameter, $h > 2a$ where a is the radius.[2] In this case, the bottom geometry can be ignored, the contact angle is near $\pi/2$, and the first mode is a planar axisymmetric motion of the free surface along a fixed node line. In most cases, this simple linear mechanical analog of the fluid motion can be used to approximate the forces and moments on the tank. Importantly for many analyses, the mechanical model usually predicts the frequency to a reasonable level of accuracy.

As the Bond number decreases below about $Bo = 1000$, the contact angle assumption must be modified and extensions to the basic potential theory must be employed. In addition, the presence of hemispherical domes or other special geometry necessitates corrections to the parameters of the equivalent mechanical model when the fluid level is near the upper or lower dome.[2] However, analytical models can still reasonably predict the sloshing parameters for Bond numbers as low as $Bo = 10$.[16]

The lateral sloshing test case is constructed in a closed domain taken as the cross section of an axisymmetric cylindrical tank having hemispherical ends. The tank radius is $a = 0.15\ \mathrm{m}$ and the barrel section length is $0.2\ \mathrm{m}$. The tank is under a static acceleration field of $g = 0.001 g_0$ and the simulated fluid lamina has a total mass of 0.1061 kg. The lattice size is $n = 346$ with a time step of $\delta\hat{t} = 2.2$ msec. Assuming that the surface tension is approximately $\hat{\sigma} = 0.0122\ \mathrm{N/m}$, the Bond number $Bo \approx 20$. At this condition, the Bond number is low enough to be simulated by the LBE and near the lower limit of the analytic prediction of the first mode natural frequency. Since both analytic and numerical models can be used to predict the sloshing response, this presents a useful verification opportunity.

The first lateral sloshing mode is excited by specifying an initial condition with the acceleration rotated $+15^\circ$ from the vertical orientation. The system is then allowed to reach a quasi-steady state condition with a total runtime of $\hat{t} = 240$ seconds. To simulate free decay, the acceleration is returned to an angle aligned with the tank symmetry axis. The free decay is simulated for $\hat{t} = 60$ seconds to capture several cycles of the very long-period fundamental lateral slosh wave. The density and lattice velocity field after $\hat{t} = 9.8$ seconds are shown in Figure 3. The time history of the force decay and spectral analysis of the domain response are shown in Figure 4. The fundamental mode is clearly visible (and appears in the frequency response) but is not dominant in frequency spectrum compared with a higher-frequency traveling-wave type free-surface mode. It is notable that the axial component of the response has a noticeable oscillation at one half the higher lateral mode frequency. These higher modes are probably an artifact of the initial conditions, which have not completely decayed, and the high-frequency response of the liquid to an instantaneous shift in the acceleration vector.

At a Bond number near $Bo = 20$, the high-g analytic solution for a right circular cylinder is a reasonable prediction for the fundamental antisymmetric mode frequency;

$$\omega_n^2 = \frac{g\lambda_n}{a} \tanh\left(\frac{\lambda_n h}{a}\right) \tag{14}$$

where λ_n are the roots of the eigenvalue equation $dJ_1(\lambda r/a)/dr = 0$ for $r = a$ and J_1 is a Bessel function of the first kind. At low Bond number and for a liquid depth of $h > 3a$, the empirical

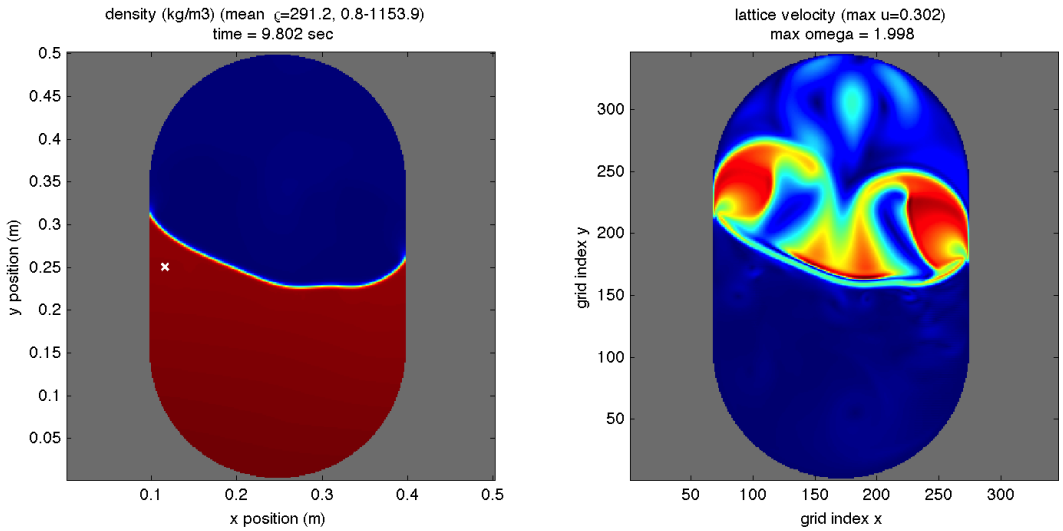

Figure 3. Lateral sloshing response after 9.8 seconds

relation* for the first mode

$$\omega_1^2 = 2.592\frac{\sigma}{\rho a^3}(1 + 0.798Bo) \tag{15}$$

correlates well with experiment; the frequency tends to increase slightly as the Bond number decreases.

The frequency also has an exact solution if the contact angle $\theta_c = \pi/2$.[2] In this case,

$$\omega_n^2 = \left[n^2\lambda_n^2\frac{\sigma}{\rho a^3} + \frac{g}{a}\right]\lambda_n \tanh\left(\frac{\lambda_n h}{a}\right). \tag{16}$$

Finally, the analytical solution corrected for the bottom geometry[16] can give an estimate of the natural frequency at this condition. The predicted and simulated frequencies are summarized in Table 1. The LBE result agrees very well with the analytical predictions.

Method	Mode $n = 1$ frequency, Hz
Equation 14	0.0552
Equation 15	0.0603
Equation 16	0.0595
Dome corrected (reference[16])	0.0551
LBE (present result)	0.0552

Table 1. Predicted sloshing natural frequencies, ~50% fill

*A typographical error appears in Equation 15 in the original reference.[2]

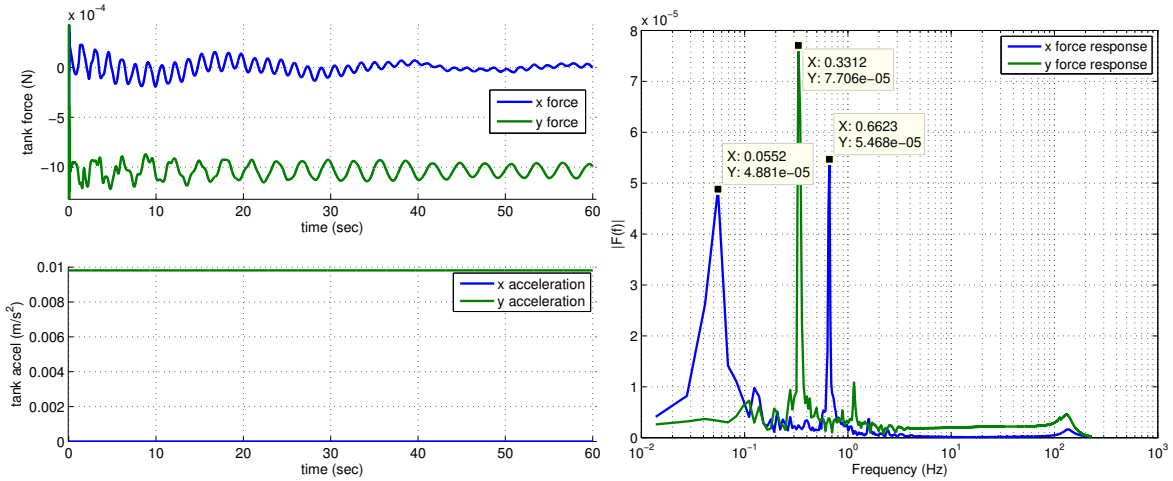

Figure 4. Time history of tank forces (left) and frequency response (right)

5 DISCUSSION AND CONCLUSIONS

It has been shown that the lattice Boltzmann method has the potential to support modeling of low Bond number flows with applications to cryogenic spacecraft propellant dynamics. Some computational and analytical advantages of the LBE have been highlighted, including data locality and explicit incorporation of an isothermal equation of state.

However, the lattice Boltzmann approach requires further study to increase its level of maturity. The LBE in the present implementation has some drawbacks that limit its scope in application to the target flow regimes. These include numerical instability for steady flow velocities exceeding about 10% of the lattice speed of sound, implicit dependence of the surface tension on the lattice parameters, and a limited ability to incorporate convective effects.

Many of these shortcomings have been addressed in the literature and can be resolved through additional development. First, the pseudopotential method provides an ability to incorporate arbitrary EoS into the model.[11] For certain species such as oxygen, other parameterized EoS may yield better accuracy over a wide range of temperatures.[17] The use of adaptive time stepping is straightforward in the LBE and has shown some promise;[18] while the Mach number of the flow is a function of the adaptive parameter, this allows larger steps to be taken when the flow is quiescent and $u \ll 1$. In this case, the accuracy may even be improved because the truncation error in the higher-order velocity terms can be kept fixed. Finally, various multi-phase thermal lattice Boltzmann techniques are emerging.[19,20]

In summary, the LBE shows promise in application to microgravity fluid flow regimes. The improvement of accuracy and stability using the aforementioned methods and the continued validation of the results using theory and test data are the subjects of future study.

REFERENCES

[1] Fisher, M., "Propellant Management in Booster and Upper Stage Propulsion Systems," Tech. Rep. TM-112924, NASA Marshall Space Flight Center, April 1997.

[2] Dodge, F., editor, *The New Dynamic Behavior of Liquids in Moving Containers*, Southwest Research Institute, 2000.

[3] Mattila, K., *Implementation Techniques for the Lattice Boltzmann Method*, Ph.D. thesis, University of Jyvaeskylae, 2010.

[4] Lallemand, P. and Luo, L., "Theory of the Lattice Boltzmann Method: Dispersion, Dissipation, Isotropy, Galilean Invariance, and Stability," Tech. Rep. CR-2000-210103, NASA Langley Research Center Institute for Computer Applications in Science and Engineering, 2000.

[5] Rettinger, C., *Fluid flow simulations using the lattice Boltzmann method with multiple relaxation times*, Master's thesis, Universtitaet Erlangen-Nuernberg, 2013.

[6] Zhen-Hua, C., Bao-Chang, S., and Lin, Z., "Simulating high Reynolds number flow in two-dimensional lid-driven cavity by multi-relaxation-time lattice Boltzmann method," *Chinese Physics*, Vol. 15, No. 8, 2006, pp. 1855.

[7] Mohamad, A. and Kuzmin, A., "A critical evaluation of force term in lattice Boltzmann method, natural convection problem," *International Journal of Heat and Mass Transfer*, Vol. 53, No. 5-6, Feb 2010, pp. 990–996.

[8] Kupershtokh, A., "New Method of incorporating a body force term into the Lattice Boltzmann Equation," *5th International EHD Workshop, Poitiers, France*, 2004.

[9] Kuzmin, A., Mohamad, A., and Succi, S., "Multi-Relaxation Time Lattice Boltzmann Model for Multiphase Flows," *International Journal of Modern Physics C*, Vol. 19, No. 06, Jun 2008, pp. 875–902.

[10] Shan, X. and Chen, H., "Lattice Boltzmann model for simulating flows with multiple phases and components," *Phys. Rev. E*, Vol. 47, No. 3, Mar 1993, pp. 1815–1819.

[11] Yuan, P. and Schaefer, L., "Equations of state in a lattice Boltzmann model," *Physics of Fluids*, Vol. 18, No. 4, 2006, pp. 042101.

[12] Kupershtokh, A., Medvedev, D., and Karpov, D., "On equations of state in a lattice Boltzmann method," *Computers & Mathematics with Applications*, Vol. 58, No. 5, Sep 2009, pp. 965–974.

[13] Carnahan, N. F., "Equation of State for Nonattracting Rigid Spheres," *The Journal of Chemical Physics*, Vol. 51, No. 2, 1969, pp. 635.

[14] Huang, H., Thorne, D., Schaap, M., and Sukop, M., "Proposed approximation for contact angles in Shan-and-Chen-type multicomponent multiphase lattice Boltzmann models," *Phys. Rev. E*, Vol. 76, No. 6, Dec 2007.

[15] Hou, S., Sterling, J., Chen, S., and Doolen, G. D., "A Lattice Boltzmann Subgrid Model for High Reynolds Number Flows," 2008.

[16] Jang, J., Alaniz, A., Yang, L., Powers, J., and Hall, C., "Mechanical Slosh Models for Rocket-Propelled Spacecraft," *AIAA Guidance, Navigation, and Control Conference*, August 2013.

[17] Duan, Z. and Hu, J., "A new cubic equation of state and its applications to the modeling of vapor-liquid equilibria and volumetric properties of natural fluids," *Geochimica et Cosmochimica Acta*, Vol. 68, No. 14, Jul 2004, pp. 2997–3009.

[18] Thuerey, N., Pohl, T., Ruede, U., Oechsner, M., and Koerner, C., "Optimization and stabilization of LBM free surface flow simulations using adaptive parameterization," *Computers and Fluids*, Vol. 35, No. 8-9, Sep 2006, pp. 934–939.

[19] He, X. and Doolen, G. D., "Thermodynamic Foundations of Kinetic Theory and Lattice Boltzmann Models for Multiphase Flows," *Journal of Statistical Physics*, Vol. 107, No. 1/2, 2002, pp. 309–328.

[20] Zhang, R. and Chen, H., "Lattice Boltzmann method for simulations of liquid-vapor thermal flows," *Phys. Rev. E*, Vol. 67, No. 6, Jun 2003, pp. 066711.